Isotropically conducting tetraaryl osmium(IV), silane, and methane molecular wire junctions

Luana Zagami,[a] Cynthia Avedian,[a] Mukund Sharma,[a] Andrew Fraire,[a] Clarissa Olivar,[a] Thomas M. Czyszczon-Burton,[a] Daniel Hernangómez-Pérez,[b,*] and Michael S. Inkpen[a,*]

[a]*Department of Chemistry, University of Southern California, Los Angeles, CA 90089, USA*

[b]*CIC nanoGUNE BRTA, Tolosa Hiribidea, 76, 20018 Donostia-San Sebastián, Spain*

E-mail: d.hernangomez@nanogune.eu, inkpen@usc.edu

ABSTRACT

Structural motifs based on tetraphenylmethane have drawn substantial interest as components of molecular electronic circuits, self-assembled monolayers, and three-dimensional polymers. When appropriately functionalized these tetratopic nodes may serve as a distinct class of *isotropic* electrical conductors, where the transport pathway is independent of connectivity. Though the functionality of these species is currently limited by the conjugation-breaking sp^3-hybridized carbon or silicon central atoms, we reasoned this could be greatly improved through exchange for a tetravalent transition metal ion; enhancing electronic coupling between the π-conjugated substituents and imparting reversible redox properties. To evaluate this hypothesis, we probe single-molecule junctions comprising oligoaryl wires with tetrahedral osmium(IV), silane, or methane centers. We find that charge transport through junctions formed from the intact organometallic species in a non-polar, inert solvent is more efficient over larger distances relative to the all-organic wires. Notably, the conductance of junctions comprising an osmium(IV) wire can also be electrochemically modulated by a factor of 47, to values 80× higher than for a silane analogue, by opening the bias window asymmetrically about the electrode Fermi level. Our experimental results are supported by first principles calculations, which predict the osmium(IV) wires can be substantially more conductive than their all-organic counterparts while also identifying specific challenges associated with modelling frozen tetraaryl compound geometries. Together, this work highlights the promising potential of transition metal tetraaryl complexes as isotropically conducting building blocks for functional circuits and extended materials.

KEYWORDS – conducting materials; DFT-NEGF; molecular electronics; single-molecule junctions; tetraaryl complexes

INTRODUCTION

In the development of molecular components that can function as electronic circuit elements such as wires or switches, most work has focused on one-dimensional (1D) species functionalized with two linker groups to establish physical and electrical connections to nanoscale electrodes.[1] This emphasis is easily rationalized given the substantial challenges[2] in moving beyond established analytical approaches based on *two-terminal* junctions formed using scanning tunneling[3,4] or conducting atomic force microscope[5] (STM or AFM), or eutectic gallium-indium (EGaIn),[6] methods. Nonetheless, several studies have also considered transport through multi-terminal,[2,7,8] or branched,[9–12] molecular junctions, for example, seeking to influence the alignment of conducting molecular orbitals with the electrode Fermi energy (E_F), or to evaluate nanoscale circuit rules governed by quantum effects. While still a distant target, we propose that extended multi-molecular circuits may, in principle, be assembled by connecting individual components through bridging molecular nodes (in addition to, for example, bridging metal nanoparticles[13] or discrete electrodes[14]). Such nodes could serve to electronically couple each element, isolate them from each other to preserve their independent function, or serve both purposes through a reversible switching event. Accordingly, efforts to develop and evaluate the conducting properties of molecular structures that could modulate transport through well-defined two- or three-dimensional (2D or 3D) geometries are critical. Such structural elements are also of current interest for the construction of conductive, permanently porous 2D and 3D ordered polymers (OPs) such as covalent organic[15] and metal-organic frameworks (COFs and MOFs),[16] materials targeted for applications in electrochemical energy storage[17,18] or chemical sensing.[19,20] Here, for example, nodes that strongly electronically-couple appended groups may be utilized in the construction of bulk materials with large band dispersions/high bulk conductivity.[16,21]

A prototypical class of 3D tetratopic building blocks are tetraphenylmethane and silane, which comprise a sp^3-hybridized carbon or silicon central atom that disrupts conjugation/coupling between each aryl arm. Such compounds, typically appended with −SH or −CN groups, have been utilized as molecular tripods on metal surfaces, and in molecular junctions.[22–33] To improve the conductivity of these materials (albeit anisotropically, see below), and to facilitate synthetic methods that yield asymmetrical tetrapods, a *spiro* carbon core structure was developed by Mayor and coworkers.[34–36] This introduces a conjugated pathway between two of the four aryl groups. The thermoelectric properties of junctions comprising different *tripodal* σ-aryl metal sulfido complexes have also been probed

computationally.[37] Concurrently, several groups have exploited building blocks based on the tetraphenylmethane or silane core, appended with appropriate coordinating or reactive groups such as $-B(OH)_2$,[38] or $-NH_2$,[39] to construct 3D OPs with extended diamond-like or distinct framework structures.[40,41] As may be expected, noting again the broken conjugation between aryl groups at each tetrahedral node, such OPs are not considered to be good bulk electrical conductors. While efforts to develop new, all-organic, π-conjugated tetratopic building blocks are underway,[42] electrically conductive 3D OPs remain rare in comparison to their 2D counterparts.[16] Notable examples include MOFs based on $Fe(tri)_2(BF_4)_x$ (tri^- = 1,2,3-triazolate, x = 0.09-0.33)[43] or FeTHQ (tetrahydroxy-1,4-quinone)[44] complexes, and a COF comprising cyclooctatetrathiophene nodes.[45] Interestingly, the conductive systems often utilize redox-active components which are thought to improve conductivity through charge hopping transport mechanisms and/or increase the number of charge carriers after partial oxidation/reduction of the system (doping).[16]

In this context, we reasoned that replacement of the sp^3-hybridized carbon or silicon atom with a transition metal ion could improve electronic coupling between aryl groups as well as imparting desirable redox properties to this family of tetratopic nodes. Of the known air-stable metal(IV) tetraaryls,[46] the osmium(IV) complexes present an particularly attractive target given their relatively well-established synthetic chemistry[47–52] and reversible redox chemistry at low potentials.[53] The frontier orbitals of these tetrahedral complexes are expected to exhibit metal-ligand π-bonding character, facilitating orbital delocalization across the central atom.[54] Recent (spectro)electrochemical studies of ferrocenyl-appended osmium(IV) tetraaryl complexes revealed spectral features attributed to intervalence-charge transfer bands in the partially oxidized species – a signature of electronic coupling between the $Fe^{2+/3+}$ centers.[48] Unfortunately, the extent of coupling across different central atoms could not be assessed in that work as the mixed-valence states of silane and methane analogues proved difficult to access. These results did, however, further motivate our efforts to evaluate charge transport through analogous compounds in comparative conductance measurements, and build on the growing interest in utilizing transition metal complexes and inorganic clusters as molecular electronic components.[55,56] While such investigations have reported, for example, extraordinary conductance-distance relationships,[57,58] exotic transport behavior such as Coulomb/current blockade,[59,60] and unusual direct metal-electrode contact chemistries,[61] they should be approached with care. Considerable synthetic challenges must often be overcome to produce an oligomeric, or modular, series of compounds, and the stability of any given complex in contact with an electrode cannot be assured.[62]

Here we synthesize and study three families of molecules comprising tetravalent osmium (**Os-*n***), silicon (**Si-*n***), and carbon (**C-*n***) centers tetrahedrally coordinated with four identical linker arms (**Figure 1a,b**). Each arm comprises a conjugated oligomeric wire with *n* = 1-3 *para*-substituted aryl units, terminated with a thioether group for electrode binding. We characterize such compounds as *isotropic* conductors, as they exhibit the same MeS−oligoaryl−M−oligoaryl−SMe transport pathway regardless of which two linker groups are connected to the electrodes (**Figure 1c**-*left*; M = Os, Si, C). This contrasts with other possible tetratopic nodes such as 1,3,6,8-substituted pyrenes, where the transport pathway changes with linker connectivity (**Figure 1c**-*right*).

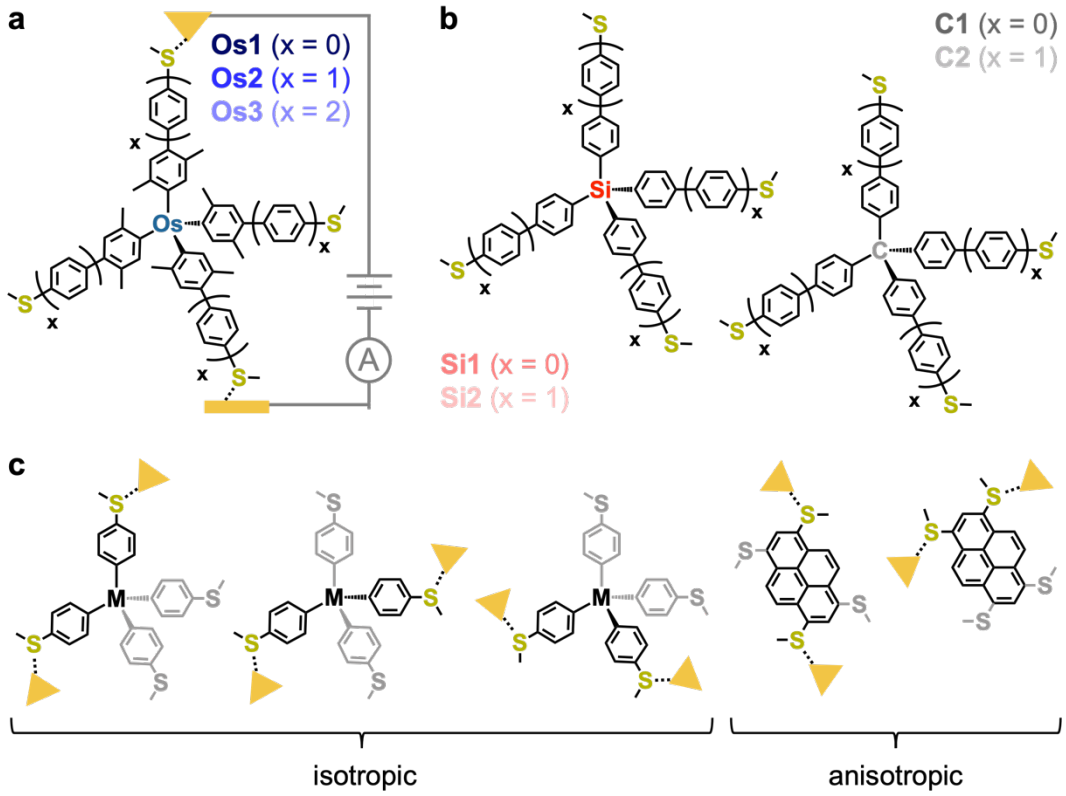

Figure 1. (a) A schematic of a single-molecule junction consisting of model tetraarylosmium(IV) complexes comprising mono, bi, or triaryl ligands terminated with thioether electrode linker groups. **(b)** Chemical structures of tetraarylsilane and tetraarylmethane analogues. **(c)** *Left:* We characterize these tetraaryl wires as *isotropic* conductors, as they comprise the same through bond conductance pathway when connected to electrodes through different linker groups (three of six possible examples illustrated; M = Os, Si, C). *Right:* In contrast, other tetratopic components such as 1,3,6,8-substituted pyrenes can exhibit different through bond conductance pathways when coordinated through different linker groups, rendering them *anisotropic* conductors (two possible examples illustrated).

Reproducible conductance measurements in tetradecane (TD) show that junctions assigned to geometries comprising intact **Os1**, **Si1**, and **C1** each exhibit a similar conductance, whereas those formed from **Os2** exhibit a conductance up to 5× higher than the all-organic wires. Given that the conductance of **Os3** junctions appears just below that of junctions comprising the much shorter **Si2** and **C2**, we conclude that the rate of tunneling decay with increasing linker arm length is smallest for the **Os-*n*** wires. In contrast to studies using TD, the conductance of intact **Os-*n*** junctions appears highly variable when formed from 1,2,4-trichlorobenzene (TCB) solutions, suggesting these complexes are particularly sensitive to the solvent environment and/or the alignment between the molecular orbitals that dominate transport and E_F. We support this hypothesis through additional measurements in propylene carbonate (PC) which show the conductance of **Os2** junctions can be modulated by 47× (through bias-dependent shifts of the transmission function relative to the average E_F of the junction), now reaching values >80× higher than junctions formed from **Si2** under the same conditions. In addition to conductance features associated with transport through the intact molecules, most measurements of **Os-*n***, **Si-*n***, and **C-*n*** wires also comprise an additional component at higher conductance. While this feature cannot yet be assigned unambiguously, we tentatively suggest it could result from junction geometries connected at one electrode through a gold aryl-π interaction, or to a dissociated linker arm bound through a Au−C(sp^2) contact. Following recent studies,[63] we recognize the requisite heterocyclic Os−, Si-, and C−aryl bond cleavage reactions may occur with loss of a stable, $[M(aryl)_3]^+$ ("trityl-like"; M = Os, Si, C) carbocation.[64]

To help rationalize our experimental findings, we perform gas-phase density functional theory (DFT) and DFT-based quantum transport calculations. These computational studies show that **Os-*n*** exhibit frontier orbitals with improved delocalization and a smaller HOMO-LUMO gap compared to **Si-*n*** and **C-*n***, consistent with solution electrochemical and UV-vis spectroscopy studies as well as expectations based-on molecular orbital theory. While the transport calculations do not fully capture the time-averaged molecular geometry and influence of solvent on level alignment, they fully support the trends observed in conductance measurements: **Os-*n*** junctions should be more conductive than their **Si-*n*** and **C-*n*** counterparts. This behavior is associated with the well-coupled frontier orbitals of the **Os-*n*** species, found at energies close to E_F. Together, our findings highlight valuable opportunities for further investigation into the measurement and computation of junctions comprising tetrahedrally coordinated complex molecules, particularly in electrochemical environments. They also motivate additional studies to refine our understanding of complex stability and frontier orbital energy alignment, addressing key challenges in the field.

RESULTS AND DISCUSSION

Synthesis and Structural Characterization

The monoaryl compounds **Os1** and **Si1** were synthesized through direct reaction between aryl magnesium bromide or aryl lithium with $(Oct_4N)_2[OsBr_6]$[47,52] or $SiCl_4$,[65] respectively, whereas **C1** was prepared through nucleophilic substitution of tetrakis(4-bromophenyl)methane with sodium thiomethoxide (**Figure 2a**).[66] The oligoaryl compounds were each prepared through Suzuki cross-coupling[51] of 4-(methylthio)phenylboronic acid or 4-(4-methylthiophenyl)phenylboronic acid with tetrakis(4-bromo-2,5-dimethylphenyl)osmium(IV),[48] tetrakis(4-bromophenyl)silane, or tetrakis(4-bromophenyl)methane. All compounds were isolated as solids that readily dissolved in common organic solvents and proved air-stable even in solution. The unoptimized yields of each product typically varied between 9-34% (55-76% per bond), except for **Si1** which was reproducibly ~2% (21% per bond) using the method described. As the compounds **Si3** and **C3** (analogous to **Os3** with Si/C central atoms) were projected to exhibit a conductance below the noise floor of our instrument, their synthesis was not pursued. While $Os(aryl)_4$ complexes are known to react with small Lewis acids such as PMe_3, isocyanides, or CO,[50] we find they do not react with the thioethers introduced here – presumably due to the steric bulk of the associated aryl group.

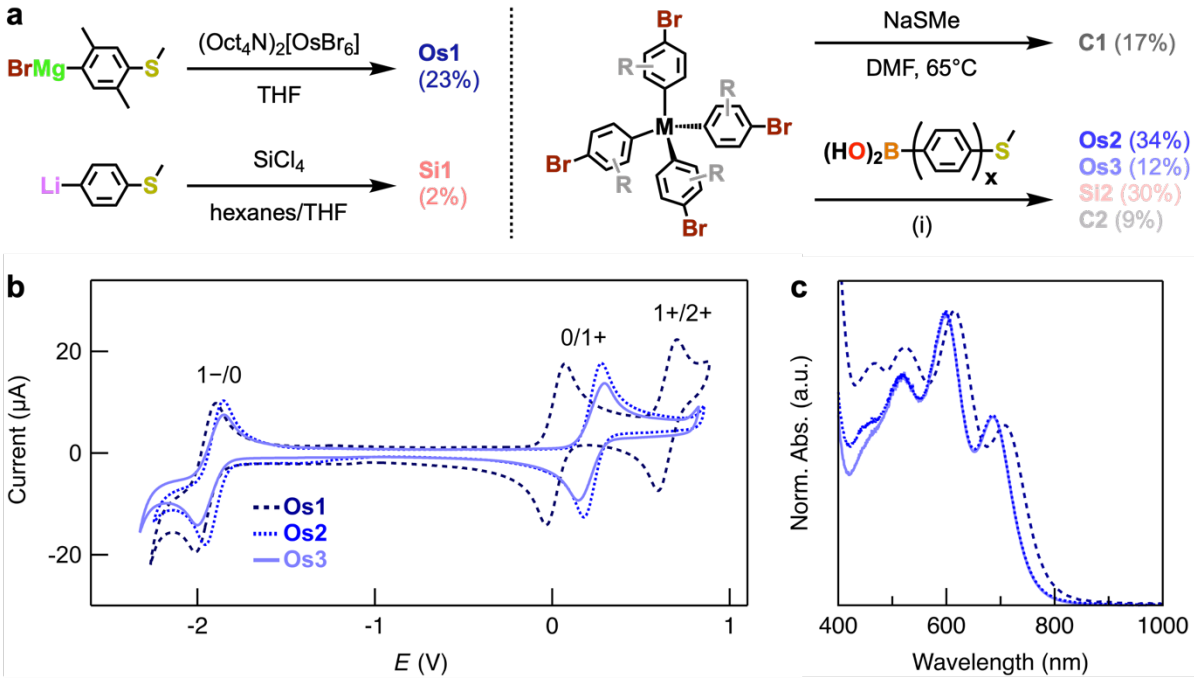

Figure 2. (a) Synthetic routes to tetraaryl compounds (x = 1, **Os2**, **Si2**, **C2**; x = 2, **Os3**). *Conditions:* (i) $Pd(PPh_3)_4$, K_2CO_3, DMF, 110°C. **(b)** Overlaid cyclic voltammograms of **Os-*n***. **(c)** Overlaid UV-vis spectra for **Os-*n***, normalized to the peak of maximum intensity in the visible region (additional spectra are provided in **Figure S1**).

The electronic properties of **Os-*n*** were probed in solution electrochemical and spectroscopic studies, given that $Os(aryl)_4$ are known to exhibit reversible redox chemistry and strongly absorb in the visible region.[48,52,53,67,68] Data for all compounds studied is provided in **Tables S1-2**. In **Figure 2b**, we plot overlaid cyclic voltammograms for **Os-*n*** in $^{n}Bu_4NPF_6$–CH_2Cl_2. These measurements reveal reversible redox features corresponding to 0/1+ and 1−/0 events ($i_{pa}/i_{pc} \sim 1$, $i_p \propto V_s^{1/2}$) which have previously been assigned to the $Os^{4+/5+}$ and $Os^{3+/4+}$ couples, respectively.[53] **Os1** also exhibits a 1+/2+ redox feature that has been observed for some other complexes with 4-substituted aryl ligands.[47,52] Notably, the electrochemical band gap of these materials (1.97-2.15 V) *increases* from **Os1** to **Os2** ~ **Os3** (with increasing linker arm length). This trend contradicts expectations for conjugated organic materials and reflects the critical role of the osmium *5d* orbitals in dictating the electronic properties of these wires. The relatively small HOMO-LUMO gap of **Os1** has previously been attributed to a high lying HOMO (in that work, referred to as "Os2-4SMe"), shifted in energy relative to the LUMO as a result of stronger resonance contributions from the pendant thioether groups.[47] In **Figure 2c**, we plot overlaid UV-vis spectra for **Os-*n*** measured in CH_2Cl_2 that each show the four strongly absorbing bands in the visible region that are characteristic of this family of complexes.[47,67,69] The trends in optical gaps (785-757 nm, 1.58-1.64 eV) correlate with those of the

electrochemical gaps, suggesting these are characteristic of the complexes themselves and are not dictated by the electrochemical environment. In contrast, **Si-*n*** and **C-*n*** (n = 1-2) exhibit optical gaps that are much larger than those of **Os-*n*** (≤335 nm, >3.7 eV) and decrease in energy with increasing linker arm length as anticipated (**Figure S1**).

The qualitative differences in electrochemical and optical gaps between the organic wires and **Os-*n*** may be readily justified. The gaps for the organic wires are expected to be relatively large due to the sp^3-hybridized central atom, which restricts π-conjugation to individual linker arms. In **Os-*n***, osmium(IV) complexes with tetrahedral geometries, the HOMO and LUMO are predicted to comprise both metal and ligand character, belonging to the orbital sets with *e* and t_2 symmetry, respectively (**Figure S18**). Here, the HOMO-LUMO gap corresponds to the tetrahedral splitting energy (Δ_{tet}), the energy difference between the *e* and t_2 levels. While the strong ligand field provided by the four σ-aryls in **Os-*n*** appears sufficient to provide a Δ_{tet} that is greater than the electron pairing energy – as evidenced by the d^4 low-spin (diamagnetic) character of these complexes – Δ_{tet} is generally considered to be smaller than the splitting energy for other common coordination geometries.[54] For example, with all else equal, $\Delta_{tet} = 4/9\Delta_{oct}$;[70] where Δ_{oct} is the octahedral splitting energy.

Conductance Measurements in Non-Polar Solvents

We next perform single-molecule conductance measurements with the STM-based break junction (STM-BJ) method, using custom-built instrumentation which has been described previously.[21,71] Briefly here, we apply a voltage (V_{bias}) between a gold STM tip and gold substrate while pushing these electrodes repeatedly in and out of mechanical contact as we measure the current (I) through the junctions that are produced. Plots of conductance ($G = I/V_{bias}$) versus increasing tip-substrate displacement reveal step features at ~1 G_0 ($= 2e^2/h$) indicative of the formation of gold-gold atomic point contacts. After breaking the point contacts in the presence of molecules that can bridge the tip-substrate nanogaps, we observe additional conductance step features below 1 G_0 that we attribute to the formation of single-molecule junctions. Thousands of such conductance-displacement traces are compiled without data selection into 1D conductance histograms, whereby the step features combine to provide peaks that can be further fit with Gaussian peaks to obtain the most probable junction conductance. The data is subjected to additional analyses, for example, by constructing 2D histograms that retain the step displacement information.

In **Figure 3a-c**, we first present overlaid 1D histograms for **Os-*n***, **Si-*n***, and **C1** measured in TD, as well as **C2** measured in TCB. Under these experimental conditions,

histograms show conductance peaks which are reproducible within a factor of ~2 (**Figures S2**, **S6b**). In most histograms, we observe two distinct peaks for each compound at high and low conductance. We associate both high and low conductance features with junctions formed from the parent compounds, given that the conductance of these peaks is found to systematically decrease as the number of aryl groups in each linker arm increases (**Figure 3e,f**). In **Figure 3d**, we present an illustrative 2D histogram for **Os2** that shows the step features corresponding to both high and low conductance junction geometries extend to ~0.5 and ~1 nm, respectively. 2D histograms for other **Os-*n***, **Si-*n***, and **C-*n*** are provided in **Figure S3** and **S6d**, which show step lengths for both high and low conductance features are similar for junctions formed from compounds with linker arms comprising the same number of aryl groups, even when these are connected to different central atoms.

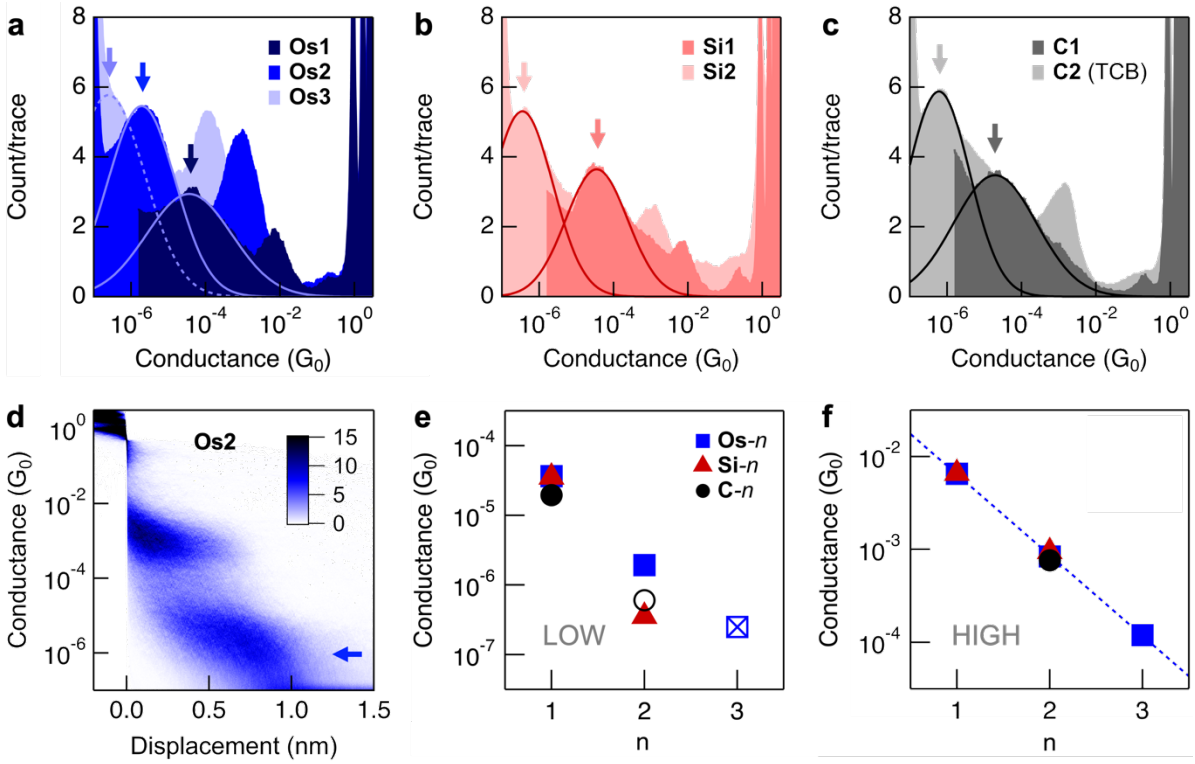

Figure 3. Overlaid 1D histograms for **(a) Os-*n***, **(b) Si-*n***, and **(c) C-*n*** (≥5,000 traces). All measurements were performed with V_{bias} = 750 mV in TD, except for studies of **Os1**, **Si1**, and **C1** which used V_{bias} = 250 mV, and **C2** which was measured in TCB. Arrows mark the low conductance features assigned to junction geometries where intact compounds are linked to each electrode by a single thioether anchor (1:1 configuration, **Figure 1a**). These are fit with Gaussian curves to obtain the most probable conductance values. **(d)** 2D conductance histogram for **Os2**. Additional 2D histograms are provided in **Figure S3**, **S6d**. **(e)** A plot of peak conductance versus *n* for the low conductance feature. All data is from measurements in TD (solid), except for **C2** which was measured in TCB (hollow). The datapoint for **Os3** (checked square) is only approximate given that the associated conductance feature is not well resolved above our instrument noise floor (dashed line fit in panel (a)). **(f)** A plot of peak conductance versus *n* for the high conductance peak feature observed in most measurements. A fit of conductance versus *n* for the high conductance peak of **Os-*n*** using $G = G_c \cdot \exp(-\beta n)$ gives $\beta = 2.0$ (dashed line).

Focusing first on the low conductance features, we note that their maximum displacement is close to the calculated S-S distance for each compound obtained from DFT-optimized structures after accounting for the gold snapback distance of ~0.6 nm.[72,73] For **Os1**, **Si1**, and **C1**, step displacement is ~0.4 nm and the calculated S-S distances are ~1.1 nm (**Figure S3**). For **Os2**, **Si2**, and **C2** the step displacement is ~1 nm and the calculated S-S distances are 1.7-1.9 nm (**Figures 3d**, **S3d**, **S6d**). Accordingly, we attribute the low conductance features to junctions comprising the intact compounds linked to each electrode by one anchor group (the

1:1 configuration; **Figure 1a**). In support of this assignment, we note the conductance observed for **Si1** (3.5×10^{-5} G_0 at V_{bias} = 250 mV in TD) is comparable to the reported conductance of the structurally similar $SiMe_2(C_6H_4\text{-}SMe)_2$ (~7×10^{-5} G_0 at V_{bias} = 225 mV in TCB; which only comprises two linker groups to form junctions).[74] While we cannot rule out the formation of junctions linked to either electrode by two or three thioether anchors, we suggest such 1:2, 1:3, or 2:2 configurations are less probable, exhibit a comparable conductance to junctions linked by a single anchor on each electrode, or are already captured in measurements at smaller junction displacements prior to breaking the molecular junction (accounting in part for the highly sloped conductance-displacement features observed).

In **Figure 3e**, a plot of peak conductance against *n* for the low conductance features reveals that the conductance of **Os1**, **Si1**, and **C1** junctions are comparable. In contrast, **Os2** junctions formed in TD exhibit a higher conductance than those of **Si2** in TD/TCB and **C2** in TCB by factors of approximately 3 to 5 – a trend that holds across repeated measurements (**Table S3**). The low conductance feature of **Os3** is not well resolved above our instrument noise floor but the most probable conductance of these junctions can be approximated (dashed fit in **Figure 3a**). Taken together, this data indicates that the decay of conductance with increasing linker arm length is shallower for **Os-*n*** than for **Si-*n*/C-*n***. These results are even more notable given that the steric influence of the methyl substituents of the 2,5-xylyl group connected to the osmium center might be expected to limit π-conjugation through the oligoaryl ligand arms by imposing a larger equilibrium aryl-aryl dihedral angle, reducing junction transport.[4] We also recognize that these methyl groups, incorporated to facilitate the synthesis and stability[75] of the **Os-*n*** complexes, will further influence the equilibrium geometry in **Os-*n*** relative to **Si-*n*/C-*n*** around the central atom (**SI**, *Geometric Analysis*), and could exert minor influences over the range of S(Me)−Au coordination geometries sampled in **Os1** junctions. Indeed, geometry optimization studies of $Si(aryl)_4$ models with and without added methyl groups (**Table S5**), as well as transmission calculations of analogous **Si2** junctions (**Figure S22**), reveal clear differences. It is therefore important to note that in the present study we strictly compare the properties of compounds having Os−2,5-xylyl, Si−phenyl, and C−phenyl central fragments, rather than probing the influence of the tetrahedrally-coordinated central atoms alone. Despite these structural intricacies, it is evident that the Os−2,5-xylyl motif maximizes transport through single-molecule junctions comprising the tetrahedrally-coordinated atoms studied.

We next comment on the important characteristics and possible origins of the high conductance peak, which is clearly observed in measurements of all compounds except for **C1**.

We plot, in **Figure 3f**, the peak conductance of this feature versus *n* for each family of compounds (see **Figure S7** for the same plot using data from TCB measurements). This analysis shows the conductance is independent of the central fragment and decreases exponentially with increasing linker arm length. A fit to the complete dataset for **Os-*n*** provides a tunneling decay constant, β, of 2.0, close to values typically found for wires with oligoaryl backbones.[4,76] Together, this strongly indicates that the junction geometry corresponding to this conductance feature contains a transport pathway dominated by the linker arm alone, independent of the central fragment. We note, in further support of this hypothesis, that the maximum displacement of each high conductance step is approximately half of the displacement observed for the low conductance step.

While the junction geometry associated with this high conductance feature cannot yet be assigned ambiguously, we propose two distinct possibilities. First, as noted above, we recognize that these tetraaryl compounds could undergo heterolytic central atom-aryl bond cleavage to provide a stable trityl (with carbon[77]) or trityl-like (with silicon[78] or osmium) cation, and a corresponding nucleophilic aryl anion. Such an anion could feasibly form junctions linked on one side through an Au−C(sp^2) bond, and on the other through the thioether (**Figure S10**). This hypothesis follows recent reports that organic wires comprising certain aryl thioethers, −SR, where R = −^{t}Bu, −CPh_3, −C_7H_7, can form junctions comprising chemisorbed S−Au linkages, apparently with loss of the stable carbocation.[63,79,80] Alternatively, the high conductance feature may be associated with junctions linked on one side by a relatively weak aryl-π interaction proximal to the central atom,[81,82] and again bound on the other side by the thioether. Further relevant discussion, data analysis, and control studies – including conductance measurements of 4'-(methylthio)-[1,1'-biphenyl]-4-yl)(triphenylphosphine)gold(I), a complex comprising the same ligand as **Os2**, **Si2**, and **C2** with a pre-installed gold-carbon bond – are provided in the **SI** (*Analysis of High Conductance Features*).

For completeness, we note that in **Figure 3c** conductance data is presented from measurements of **C2** in TCB because studies of this molecule in TD have so far not provided the expected low conductance peak (**Figure S4**). We suggest this feature is either too low in conductance and/or sloped in TD to resolve above our noise floor. While this result could be interpreted as an indication that this molecule rapidly decomposes at the interface, forming a highly stable [C(biphenyl−SMe)]$^+$ carbocation (see **Figure S10** and above discussion),[63,79] this would appear inconsistent with our other findings. Both low and high conductance features *are* observed in measurements of **Si2** in TD, a molecule which should form a carbocation of similar

stability. Furthermore, the methane-based compounds do not appear to exhibit a particularly high rate of interfacial decomposition given that high conductance features are not observed in measurements of **C1** in TD (which in this scenario would correspond to junction geometries comprising dissociated ligand arms).

Although measurements of **C2** in TCB proved useful, we caution that low conductance junctions of **Os-*n*** measured in TCB (a widely utilized solvent for single-molecule conductance experiments) exhibit significant experiment-to-experiment conductance variation. As illustrated by the examples provided in **Figure S5**, the low conductance feature of **Os2** varies by a factor of ~8, up to 1.4×10^{-5} G_0 (an order of magnitude higher than the conductance measured in TD). In some experiments, it appears that **Os3** junctions of the 1:1 configuration can be clearly resolved above our instrument noise floor. We hypothesize that the observed conductance variation results from changes in conducting orbital-E_F energy level alignment (supported through additional experiments and DFT calculations presented below), or partial *in situ* oxidation of **Os-*n*** junctions in TCB. While a complete rationalization of the influence of solvent environment on the conductance of **Os-*n*** junctions lies beyond the scope of this work, we note that the use of TCB does have the potential to complicate studies of chemically sensitive or redox-active compounds (particularly under applied electric fields at or near the junction). For example, aromatic chlorinated solvents are known to interact with a gold surface to a limited degree, influencing level alignment.[83] Other chlorinated solvents such as $CDCl_3$ or CH_2Cl_2 can prove weakly acidic due to the photogeneration of HCl,[84] or may oxidize compounds with low redox potentials such as ferrocene through charge transfer to solvent (CTTS) optical transitions.[85] Interestingly in this context, absorption spectra of **Os2** in CH_2Cl_2, TCB, and TD do not exhibit significant differences that might prove indicative of bulk protonation or oxidation (**Figure S1c**). Nonetheless, in contrast to studies in TCB, the greater consistency of **Os-*n*** conductance measurements in TD may be readily attributed to the non-polar, inert character of this solvent, which inhibits the dissolution of charged species and does not strongly interact with the gold surface.

*Tuning the Conductance of **Os2** in a Polar Solvent*

To help further assess the potential for **Os-*n*** junctions to vary in conductance with level alignment, we perform additional conductance measurements of **Os2** in a third solvent, propylene carbonate (PC). In such experiments, it is essential to use a wax-coated tip to minimize background Faradaic and capacitive currents that would otherwise obscure junction tunneling currents of interest.[86] However, as the exposed tip electrode area (~1 μm) is small

relative to the area of the substrate electrode (~1 cm^2), this also results in the generation of a dense double-layer at the tip that is understood to induce a bias-dependent shift of the transmission function relative to the average E_F of the junction.[87] As a result, the bias window opens asymmetrically about E_F, enabling experiments that probe the transmission landscape for different molecules,[87] establish whether the dominant conducting orbital is occupied or unoccupied,[87,88] or construct junctions that exhibit significant current rectification.[89]

In **Figure 4a** and **b** we present overlaid 1D histograms obtained for measurements of **Os2** in PC with no added electrolyte at different tip biases, across two separate experiments. The conductance of the feature assigned to intact **Os2** junctions significantly increases as the tip bias is made more positive. These changes are quantified by fitting this peak in each histogram with a Gaussian curve, which reveals that the most probable conductance of the intact junctions can be modulated by a factor of 47. In **Figure 4c**, we summarize these results by plotting the obtained peak conductance values against the applied tip bias. Importantly, this plot also highlights the reproducibility of conductance values at a given tip bias between different experiments. Representative 2D histograms, presented in **Figure 4d** and **e**, show that the maximum junction displacements of the lower conductance features are comparable to that found in TD measurements (**Figure 3d**) and do not significantly vary with changing tip bias (additional 2D histograms are plotted in **Figure S11**). This further supports our assignment of this electrochemically modulated histogram component to the intact junction. In **Figure 4f**, we provide a cyclic voltammogram of **Os2** obtained *in situ* using the gold STM tip as working electrode and the substrate as both reference and counter electrode (obtained during experiment 2, shown in **Figure 4b**). This reveals a redox wave close to ~0.8 V, which is observed at approximately +0.65 V relative to the $Fe^{2+/3+}$ couple of ferrocene measured under the same conditions (**Figure S12**). As this feature is not observed in the absence of **Os2** we associate it with the 0/1+ event characteristic of this compound, albeit shifted by +400 mV relative to measurements in $^{n}Bu_4NPF_6$-CH_2Cl_2 (**Figure 2b**). This indicates that we approach the HOMO resonance as we apply a more positive bias to the tip. We find that we cannot easily form junctions for tip biases greater than +700 mV; similar limits have been observed in studies of other molecules with resonances close to E_F.[87]

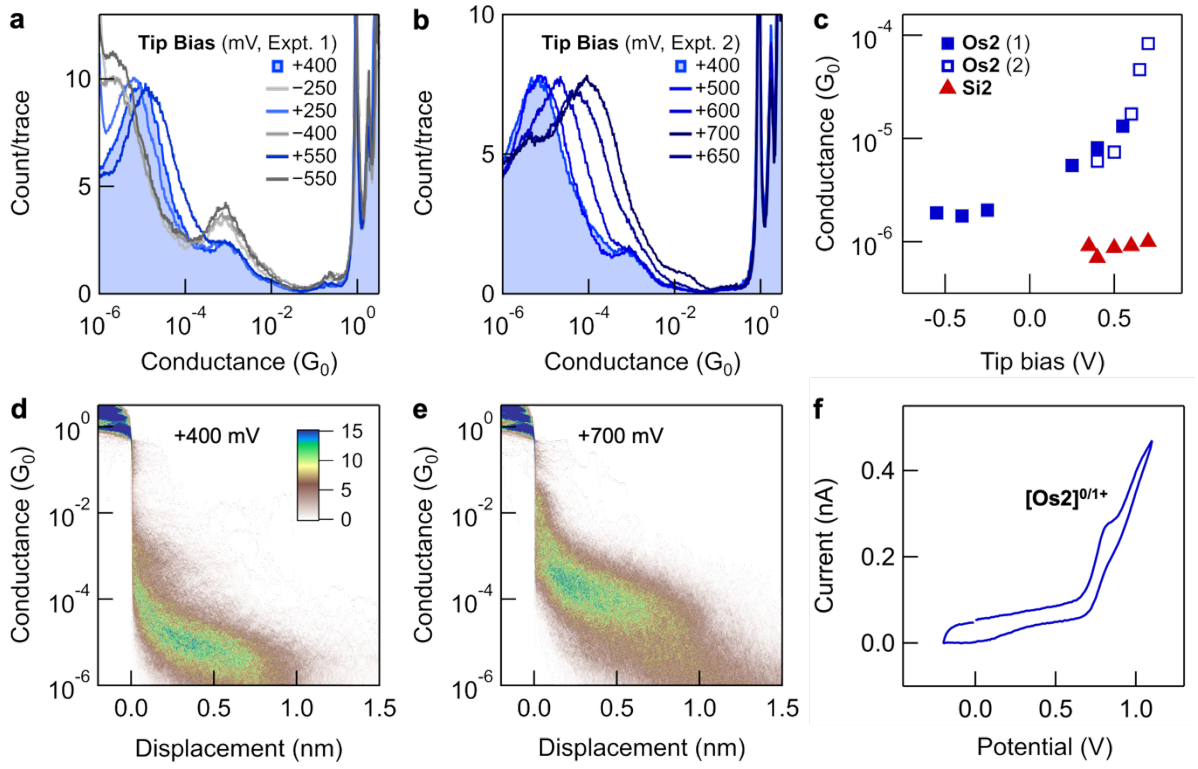

Figure 4. (a,b) Overlaid 1D histograms (2,000 traces) for measurements of **Os2** in PC at different tip biases, across two different experiments (biases listed in order of measurement). This data shows that junction conductance can increase by a factor of 47 with changing tip bias. **(c)** A plot of peak conductance versus tip bias for the measurements of **Os2** shown in panels (a) and (b) (blue). An overlaid plot for PC measurements of **Si2** show these junctions exhibit a much smaller dependance on tip bias (red; see **Figure S13** for corresponding histograms). **(d,e)** 2D histograms obtained for measurements at tip bias = +400 mV and +700 mV, respectively, corresponding to the 1D histograms in panel (b). Additional 2D histograms corresponding to the 1D histograms in panel (a) are provided in **Figure S11**. **(f)** Cyclic voltammogram obtained using the same tip, substrate, and solution as used for the STM-BJ measurements in panel (b) with an external potentiostat. Here the wax-coated STM tip served as the working ultramicroelectrode, the substrate as both the counter and reference electrodes. Additional voltammograms are provided in **Figure S12**.

These observations indicate that intact **Os2** junctions exhibit a sloped transmission function near E_F, with transport dominated by the occupied states,[87] as is also found in the calculations discussed below. Critically, comparison studies that track the low conductance feature of intact **Si2** junctions, as well as the high conductance peak in both **Os2** and **Si2** measurements, show a much smaller or insignificant change in conductance with tip bias, respectively (**Figure 4a-c, S13**). This result is consistent with a transmission function that is relatively flat around E_F. We also note that the high conductance feature reduces in intensity as the tip bias is made more positive in measurements of **Os2** and appears similarly suppressed at

positive tip biases in measurements of **Si2**. Such molecule-specific variations in peak intensity with changing tip bias in PC have been observed in previous reports,[87] rendering the origin of the observed changes for these compounds ambiguous. Overall, these studies support the view that variations in level alignment could indeed result in significant changes to the conductance of intact **Os-*n*** junctions on the order of those observed in repeated measurements in TCB, while not strongly affecting transport through intact **Si2** junctions or the geometries associated with high conductance features. At tip bias = +700 mV, the conductance of **Os2** junctions is 83× larger smaller than that of those formed from **Si2**, definitively illustrating the distinct electronic structures of these structurally analogous compounds.

Computational Analyses of Model Systems in the Gas Phase

To gain further insight into the electronic properties of these junctions, we now turn to quantum transport calculations. Our calculations are based on density functional theory (DFT) and the non-equilibrium Green's functions formalism, and are performed using the combination of FHI-aims[90] and the transport module AITRANSS.[91–94] Additional computational details can be found in the **SI**. We show, in **Figure 5a**, overlaid transmission functions for **Os-*n*** junctions, bound to gold electrodes with two thioether linkers. An example of these relaxed junction geometries is given in **Figure 5c**. We observe that the conductance, which is proportional to the transmission at E_F, is highest for the smallest complex and follows the trend: **Os1** > **Os2** > **Os3**. This behavior appears counterintuitive when considering the trend observed in the HOMO-LUMO gaps for the isolated molecules (see **Table S8** for calculated values, which qualitatively agree with those found through experiment), and in which shorter wires typically exhibit larger HOMO-LUMO gaps. Here, the conductance ordering is attributed to the alignment of the HOMO level with E_F, along with its decreasing width as the wire length increases. As is common in calculations using semi-local functionals (here, PBE[95]), the computed conductance of **Os-*n*** junctions is overestimated by more than an order of magnitude compared to experiment, a well-understood artifact arising from the limitations of generalized-gradient approximations to DFT functionals.[96,97] Notably, the calculated conductance for **Os3** is low, consistent with experimental observations that it almost falls below our instrumental noise floor.

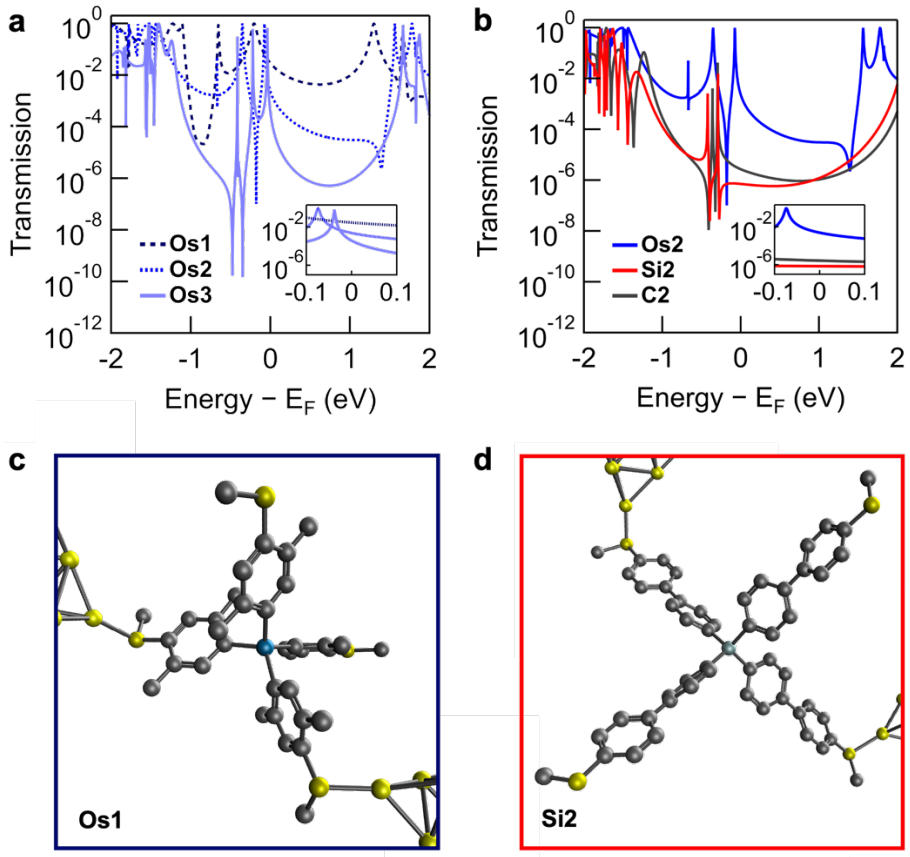

Figure 5. (a) Overlaid transmission functions for the **Os-*n*** series. **(b)** Comparison of overlaid transmission functions for **Os2**, **Si2**, and **C2** (data for **Os2** reproduced from panel (a)). Insets provide an expanded view of transmission close to the Fermi level. **(c-d)** Optimized geometries of **Os1** and **Si2** junctions, respectively. Hydrogen atoms excluded for clarity.

We have also performed quantum transport calculations for the **Si-*n*** and **C-*n*** molecular junction series. In **Figure 5b**, we show a comparison of the transmission functions for $n = 2$ (**Os2**, **Si2**, **C2**), additional results for the entire **Si-*n*** and **C-*n*** series are available in **Figure S21**. An example of one of these relaxed junction geometries is shown in **Figure 5d**. We recognize that all these junctions exhibit complex transmission functions with Fano-type interference features, which can be attributed to the existence of non-bonded aryl groups in the complexes. The role of non-bonded side groups not directly involved in the main transmission pathway in generating quantum interference effects is well established.[98,99] In the case of the **Si2** junction, we have checked this effect by removing the two non-bonded aryl arms and substituting them with $–CH_3$ groups (**Figure S22**). This modification leads to the disappearance of the Fano-type resonances close to E_F. The calculated conductance of **Si-*n*** and **C-*n*** junctions follows the same trend as for **Os-*n***, with **Si1** > **Si2** > **Si3** and the same ordering for **C-*n***. However, in this case, the trend aligns with the expected behavior based on the HOMO-LUMO gaps, indicating that

these molecules, in general, behave as conventional molecular wires. Additionally, the calculated HOMO-LUMO gaps of **Si-*n*** and **C-*n*** are very similar and substantially larger than those of **Os-*n*** with a difference of 1–2 eV between **Os-*n*** and **Si-*n*/C-*n*** (**Table S8**).

Our transport calculations show that **Os2** junctions are HOMO conducting and exhibit a significantly higher conductance than junctions formed from **Si2/C2**, though the exact difference may change due differences in E_F alignment and solvent effects (as noted below). This qualitatively aligns with our experimental studies in PC which show that the conductance of intact **Os2** junctions can vary by a factor up to ~80 relative to their **Si2** analogues. Our calculations for **Si2** also recover the flatness of the transmission function close to E_F as suggested by these conductance measurements. The trend is further supported by the orbital character of the HOMO in **Os-*n*** which shows greater density on the central atom (Os d_z^2) compared to the sp^3-like character in **Si-*n*** or **C-*n*** (see, an example, in **Figure S17**). This facilitates delocalization of the thioanisole π-system and contributes to the higher conductance observed in **Os-*n***. Finally, it is important to stress that our calculations do not account for the effects of solvents or electrochemical influences. This limitation could offer a possible explanation for some discrepancies between the theoretical results and experimental observations.

In closing, we also note that we have calculated PBE-based tunnel couplings, which are related to conductance.[4,100] The results of these calculations align well with the DFT transmission calculations in **Figure 5**, consistently recovering highly conductive **Os-*n*** junctions (**SI**, *Tunnel Coupling*). The tunnel coupling values also indicate that variations in the calculated conductance may result from the orientation of adjacent aryl rings connected through the central atom (explicitly defined, in **Figure S15**, using pairs of dihedral angles). While variations due to non-equivalent geometries can also be reproduced in transmission calculations (**Figure S23**), these do not change the conductance ordering **Os-*n*** > **Si-*n*** ~ **C-*n***. To assess the sensitivity of transport predictions and conductance ordering to the choice of exchange-correlation functional, we also performed tunnel coupling calculations using the hybrid functional B3LYP. Tunnel coupling calculations are well suited to hybrid functionals, which should otherwise always be avoided in systems with many gold atoms, as they misrepresent the electronic structure near E_F.[101] We reemphasize that tunnel coupling and full *ab initio* transport calculations show good agreement in capturing the conductance trends, as exemplified by the PBE-based comparison discussed above. Interestingly, the B3LYP-based tunnel coupling calculations suggest that the differences between **Os-*n***, **Si-*n***, and **C-*n*** junctions may be smaller than those predicted by PBE (**Table S6,7**), in better agreement with

experimental trends and providing further insight into the influence of exchange-correlation effects on transport properties.

CONCLUSION

We have shown, through a combination of experiment and DFT-based calculations, that the conductance of single-molecule junctions formed from charge neutral osmium(IV) tetraaryl compounds can be significantly larger than analogues comprising analogous tetrahedral silane or methane nodes. This provides the first clear evidence in support of the potential utility of these organometallic compounds to form 3D OPs with improved conductivity relative to their all-organic congeners. The variability of **Os-*n*** measurements in TCB, the highly tunable conductance of **Os2** junctions in PC (relative to **Si2**), and the sloped character of their calculated transmission functions near E_F further reveal that the conductance of the intact organometallic wire junctions is particularly sensitive to the local (electro)chemical environment. More broadly, this highlights the important role that the solvent environment plays in obtaining reproducible conductance measurements of compounds such as **Os-*n*** – systems having well coupled frontier orbitals proximal to E_F and and/or (electrochemically) reactive potential. Solution-based electrochemical and spectroscopic measurements of the molecular species studied here, as well as computational simulations, corroborate the observed transport behavior, clearly showing that **Os-*n*** exhibit smaller HOMO-LUMO gaps than **Si-*n*** or **C-*n***. Importantly, our analysis of these trends suggest that transport through coordination complexes with appropriate electronic structure can be readily modulated through adjustments to the ligand field, where the resulting changes to Δ are commensurate with changing the HOMO-LUMO gap.

Remarkably, for most molecules studied in TD, we also find evidence for high conductance junctions comprising a distinct gold aryl-π interaction or Au−C(sp^2) contact chemistry following loss of a stable trityl-like cation. Considering the latter possibility, we note that the installation of linker precursors comprising stable leaving groups could provide practical strategies to form other chemisorbed junction contact chemistries of interest (beyond Au−S). Taken together, these results underscore the potential of osmium(IV) tetraaryl complexes for applications requiring efficient through-molecule charge transport while also demonstrating the need for further investigation into their stability during measurements between gold electrodes. Despite exhibiting a remarkable air-stability in solution, these compounds are known to undergo a range of reactions *ex situ* to form, for example, products

comprising oxo or η^6-biaryl ligands, including $OsO(aryl)_4$,[68] $OsO_2(aryl)_2$,[102] or $Os(\eta^6\text{-biaryl})(aryl)_2(L)$ (previously isolated with L = PMe_3, CO).[50] Conductance measurements of different osmium σ-aryl species synthesized *ex situ* should be pursued to assess the possibility of their formation *in situ*. Future studies that probe the conductance of **Os-*n*** and other tetraaryl complexes in different charge states are expected to provide additional important insights.

ASSOCIATED CONTENT

Electronic Supplementary Information (ESI) available: Additional synthetic, spectroscopic, conductance, and computational details and data. This includes synthetic procedures, 1D and 2D conductance histograms, transmission calculations, and ^1H and $^{13}C\{^1H\}$ NMR spectra for all new compounds.

AUTHOR INFORMATION

Corresponding Author

Michael S. Inkpen – Email: inkpen@usc.edu
Daniel Hernangómez-Pérez – Email: d.hernangomez@nanogune.eu

Notes

The authors declare no competing financial interest.

ACKNOWLEDGEMENTS

This work was primarily supported by funding from the University of Southern California (USC) and the National Science Foundation (NSF CAREER Award to M.S.I., CHE-2239614). D. H.-P. is grateful for funding from the Diputación Foral de Gipuzkoa through Grants 2023-FELL-000002-01, 2024-FELL-000009-01. D. H.-P. acknowledges the technical and human support provided by the DIPC Supercomputing Center. Instrumentation in the USC Chemistry Instrument Facility was acquired with support from the USC Research and Innovation Instrumentation Award Program. Additionally, funds provided by the NSF (DBI-0821671, CHE-0840366) and National Institutes of Health (S10 RR25432) supported the acquisition of the NMR spectrometers used in our work.

REFERENCES

(1) Su, T. A.; Neupane, M.; Steigerwald, M. L.; Venkataraman, L.; Nuckolls, C. Chemical Principles of Single-Molecule Electronics. *Nature Rev. Mater.* **2016**, *1* (3), 16002. https://doi.org/10.1038/natrevmats.2016.2.

(2) Xiang, D.; Jeong, H.; Kim, D.; Lee, T.; Cheng, Y.; Wang, Q.; Mayer, D. Three-Terminal Single-Molecule Junctions Formed by Mechanically Controllable Break Junctions with Side Gating. *Nano Lett.* **2013**, *13* (6), 2809–2813. https://doi.org/10.1021/nl401067x.

(3) Xu, B.; Tao, N. J. Measurement of Single-Molecule Resistance by Repeated Formation of Molecular Junctions. *Science* **2003**, *301* (5637), 1221–1223.

(4) Venkataraman, L.; Klare, J. E.; Nuckolls, C.; Hybertsen, M. S.; Steigerwald, M. L. Dependence of Single-Molecule Junction Conductance on Molecular Conformation. *Nature* **2006**, *442* (7105), 904–907. http://www.nature.com/nature/journal/v442/n7105/suppinfo/nature05037_S1.html.

(5) Wold, D. J.; Frisbie, C. D. Formation of Metal-Molecule-Metal Tunnel Junctions: Microcontacts to Alkanethiol Monolayers with a Conducting AFM Tip. *J. Am. Chem. Soc.* **2000**, *122*, 2970–2971.

(6) Chiechi, R. C.; Weiss, E. A.; Dickey, M. D.; Whitesides, G. M. Eutectic Gallium–Indium (EGaIn): A Moldable Liquid Metal for Electrical Characterization of Self-Assembled Monolayers. *Angew. Chem. Int. Ed.* **2008**, *47* (1), 142–144. https://doi.org/10.1002/anie.200703642.

(7) Fu, H.; Zhu, X.; Li, P.; Li, M.; Yang, L.; Jia, C.; Guo, X. Recent Progress in Single-Molecule Transistors: Their Designs, Mechanisms and Applications. *J. Mater. Chem. C* **2022**, *10* (7), 2375–2389. https://doi.org/10.1039/D1TC04079K.

(8) Neuhauser, D.; Baer, R. Phase Coherent Electronics: A Molecular Switch Based on Quantum Interference. *J. Am. Chem. Soc.* **2002**, *124* (16), 4200–4201.

(9) Vazquez, H.; Skouta, R.; Schneebeli, S.; Kamenetska, M.; Breslow, R.; Venkataraman, L.; Hybertsen, M. S. Probing the Conductance Superposition Law in Single-Molecule Circuits with Parallel Paths. *Nature Nanotechnol.* **2012**, *7* (10), 663–667. http://www.nature.com/nnano/journal/v7/n10/abs/nnano.2012.147.html

(10) Magoga, M.; Joachim, C. Conductance of Molecular Wires Connected or Bonded in Parallel. *Phys Rev B Solid State* **1999**, *59* (24), 16011–16021.

(11) Błaszczyk, A.; Chadim, M.; von Hänisch, C.; Mayor, M. Synthesis of Macrocyclic Molecular Rods as Potential Electronic Devices. *Eur J Org Chem* **2006**, *2006* (17), 3809–3825. https://doi.org/10.1002/ejoc.200600336.

(12) Wilson, L. E.; Yue, T. T. C.; Inkpen, M. S.; Grace, I.; White, A. J. P.; Lambert, C.; Albrecht, T.; Long, N. J. Controlling Quantum Interference Patterns in Redox-Active Rings. *J. Organomet. Chem.* **2024**, *1022*, 123368. https://doi.org/10.1016/j.jorganchem.2024.123368.

(13) Cui, X. D.; Primak, A.; Zarate, X.; Tomfohr, J.; Sankey, O. F.; Moore, A. L.; Moore, T. A.; Gust, D.; Harris, G.; Lindsay, S. M. Reproducible Measurement of Single-Molecule Conductivity. *Science* **2001**, *294* (5542), 571–574. https://doi.org/10.1126/science.1064354.

(14) Byeon, S. E.; Kang, H.; Yoon, H. J. Toward Printed Molecular Electronics: Direct Printing of Liquid Metal Microelectrode on Self-Assembled Monolayers. *Adv. Electron. Mater.* **2021**, *7* (2), 2000829. https://doi.org/10.1002/aelm.202000829.

(15) Jin, E.; Asada, M.; Xu, Q.; Dalapati, S.; Addicoat, M. A.; Brady, M. A.; Xu, H.; Nakamura, T.; Heine, T.; Chen, Q.; Jiang, D. Two-Dimensional Sp2 Carbon–Conjugated Covalent Organic Frameworks. *Science* **2017**, *357* (6352), 673–676.

(16) Xie, L. S.; Skorupskii, G.; Dincă, M. Electrically Conductive Metal–Organic Frameworks. *Chem. Rev.* **2020**, *120* (16), 8536–8580. https://doi.org/10.1021/acs.chemrev.9b00766.
(17) Zhang, Y.; Riduan, S. N.; Wang, J. Redox Active Metal- and Covalent Organic Frameworks for Energy Storage: Balancing Porosity and Electrical Conductivity. *Chem. Eur. J.* **2017**, *23* (65), 16419–16431. https://doi.org/10.1002/chem.201702919.
(18) Calbo, J.; Golomb, M. J.; Walsh, A. Redox-Active Metal–Organic Frameworks for Energy Conversion and Storage. *J. Mater. Chem. A* **2019**, *7* (28), 16571–16597. https://doi.org/10.1039/C9TA04680A.
(19) Kreno, L. E.; Leong, K.; Farha, O. K.; Allendorf, M.; Van Duyne, R. P.; Hupp, J. T. Metal–Organic Framework Materials as Chemical Sensors. *Chem. Rev.* **2012**, *112* (2), 1105–1125. https://doi.org/10.1021/cr200324t.
(20) Meng, Z.; Stolz, R. M.; Mendecki, L.; Mirica, K. A. Electrically-Transduced Chemical Sensors Based on Two-Dimensional Nanomaterials. *Chem. Rev.* **2019**, *119* (1), 478–598. https://doi.org/10.1021/acs.chemrev.8b00311.
(21) Miao, Z.; Quainoo, T.; Czyszczon-Burton, T. M.; Rotthowe, N.; Parr, J. M.; Liu, Z.; Inkpen, M. S. Charge Transport across Dynamic Covalent Chemical Bridges. *Nano Lett* **2022**, *22* (20), 8331–8338. https://doi.org/10.1021/acs.nanolett.2c03288.
(22) Šebera, J.; Lindner, M.; Gasior, J.; Mészáros, G.; Fuhr, O.; Mayor, M.; Valášek, M.; Kolivoška, V.; Hromadová, M. Tuning the Contact Conductance of Anchoring Groups in Single Molecule Junctions by Molecular Design. *Nanoscale* **2019**, *11* (27), 12959–12964. https://doi.org/10.1039/c9nr04071d.
(23) Valášek, M.; Mayor, M. Spatial and Lateral Control of Functionality by Rigid Molecular Platforms. *Chem. Eur. J.* **2017**, *23* (55), 13538–13548. https://doi.org/10.1002/chem.201703349.
(24) Yao, Y.; Tour, J. M. Facile Convergent Route to Molecular Caltrops. *J. Org. Chem.* **1999**, *64* (6), 1968–1971. https://doi.org/10.1021/jo982085g.
(25) Zhu, L.; Harima, Y.; Yamashita, K.; Tang, H.; Hirayama, D.; Aso, Y.; Otsubo, T. Electrochemical Properties of Self-Assembled Monolayers of Tripod-Shaped Molecules and Their Applications to Organic Light-Emitting Diodes. *Chem. Commun.* **2001**, No. 18, 1830–1831. https://doi.org/10.1039/b105922j.
(26) Hirayama, D.; Takimiya, K.; Aso, Y.; Otsubo, T.; Hasobe, T.; Yamada, H.; Imahori, H.; Fukuzumi, S.; Sakata, Y. Large Photocurrent Generation of Gold Electrodes Modified with [60]Fullerene-Linked Oligothiophenes Bearing a Tripodal Rigid Anchor. *J. Am. Chem. Soc.* **2002**, *124* (4), 532–533. https://doi.org/10.1021/ja016703d.
(27) Wei, L.; Padmaja, K.; Youngblood, W. J.; Lysenko, A. B.; Lindsey, J. S.; Bocian, D. F. Diverse Redox-Active Molecules Bearing Identical Thiol-Terminated Tripodal Tethers for Studies of Molecular Information Storage. *J. Org. Chem.* **2004**, *69* (5), 1461–1469. https://doi.org/10.1021/jo0349476.
(28) Wei, L.; Tiznado, H.; Liu, G.; Padmaja, K.; Lindsey, J. S.; Zaera, F.; Bocian, D. F. Adsorption Characteristics of Tripodal Thiol-Functionalized Porphyrins on Gold. *J. Phys. Chem. B* **2005**, *109* (50), 23963–23971. https://doi.org/10.1021/jp0537005.
(29) Ie, Y.; Hirose, T.; Yao, A.; Yamada, T.; Takagi, N.; Kawai, M.; Aso, Y. Synthesis of Tripodal Anchor Units Bearing Selenium Functional Groups and Their Adsorption Behaviour on Gold. *Phys Chem Chem Phys* **2009**, *11* (25), 4949–4951. https://doi.org/10.1039/b906286f.
(30) Lindner, M.; Valášek, M.; Homberg, J.; Edelmann, K.; Gerhard, L.; Wulfhekel, W.; Fuhr, O.; Wächter, T.; Zharnikov, M.; Kolivoška, V.; Pospíšil, L.; Mészáros, G.; Hromadová, M.; Mayor, M. Importance of the Anchor Group Position (Para versus

Meta) in Tetraphenylmethane Tripods: Synthesis and Self-Assembly Features. *Chem. Eur. J.* **2016**, *22*, 13218–13235. https://doi.org/10.1002/chem.201602019.
(31) Valášek, M.; Lindner, M.; Mayor, M. Rigid Multipodal Platforms for Metal Surfaces. *Beilstein J. Nanotechnol.* **2016**, *7* (1), 374–405. https://doi.org/10.3762/bjnano.7.34.
(32) Sebechlebská, T.; Šebera, J.; Kolivoška, V.; Lindner, M.; Gasior, J.; Mészáros, G.; Valášek, M.; Mayor, M.; Hromadová, M. Investigation of the Geometrical Arrangement and Single Molecule Charge Transport in Self-Assembled Monolayers of Molecular Towers Based on Tetraphenylmethane Tripod. *Electrochim. Acta* **2017**, *258*, 1191–1200. https://doi.org/10.1016/j.electacta.2017.11.174.
(33) Kolivoška, V.; Šebera, J.; Sebechlebská, T.; Lindner, M.; Gasior, J.; Mészáros, G.; Mayor, M.; Valášek, M.; Hromadová, M. Probabilistic Mapping of Single Molecule Junction Configurations as a Tool to Achieve the Desired Geometry of Asymmetric Tripodal Molecules. *Chem. Commun.* **2019**, *55* (23), 3351–3354. https://doi.org/10.1039/c8cc09681c.
(34) Šebera, J.; Kolivoška, V.; Valášek, M.; Gasior, J.; Sokolová, R.; Mészáros, G.; Hong, W.; Mayor, M.; Hromadová, M. Tuning Charge Transport Properties of Asymmetric Molecular Junctions. *J. Phys. Chem. C* **2017**, acs.jpcc.7b01105. https://doi.org/10.1021/acs.jpcc.7b01105.
(35) Karimi, M. A.; Bahoosh, S. G.; Valášek, M.; Bürkle, M.; Mayor, M.; Pauly, F.; Scheer, E.; Agraït, N.; Cuevas, J. C.; Mikkelsen, K. V. Identification of the Current Path for a Conductive Molecular Wire on a Tripodal Platform. *Nanoscale* **2016**, *8* (20), 10582–10590. https://doi.org/10.1039/C5NR08708B.
(36) Gerhard, L.; Edelmann, K.; Homberg, J.; Valášek, M.; Bahoosh, S. G.; Lukas, M.; Pauly, F.; Mayor, M.; Wulfhekel, W. An Electrically Actuated Molecular Toggle Switch. *Nature Commun.* **2017**, *8*, 14672.
(37) Al-Owaedi, O. A.; Najeeb, H. N.; Aldulaimi, A. K. O.; Alwan, N. H.; Ali, M. S.; Dwech, M. H.; AL-Da'amy, M. A. Thermoelectric Signature of D-Orbitals in Tripod-Based Molecular Junctions. *Mater. Adv.* **2024**, 10.1039.D4MA00646A. https://doi.org/10.1039/D4MA00646A.
(38) El-Kaderi, H. M.; Hunt, J. R.; Mendoza-Cortés, J. L.; Côté, A. P.; Taylor, R. E.; O'Keeffe, M.; Yaghi, O. M. Designed Synthesis of 3D Covalent Organic Frameworks. *Science* **2007**, *316* (5822), 268–272. https://doi.org/10.1126/science.1139915.
(39) Uribe-Romo, F. J.; Hunt, J. R.; Furukawa, H.; Klöck, C.; O'Keeffe, M.; Yaghi, O. M. A Crystalline Imine-Linked 3-D Porous Covalent Organic Framework. *J. Am. Chem. Soc.* **2009**, *131* (13), 4570–4571. https://doi.org/10.1021/ja8096256.
(40) Zaręba, J. K. Tetraphenylmethane and Tetraphenylsilane as Building Units of Coordination Polymers and Supramolecular Networks – A Focus on Tetraphosphonates. *Inorg. Chem. Commun.* **2017**, *86*, 172–186. https://doi.org/10.1016/j.inoche.2017.10.013.
(41) Guan, X.; Chen, F.; Fang, Q.; Qiu, S. Design and Applications of Three Dimensional Covalent Organic Frameworks. *Chem. Soc. Rev.* **2020**, *49* (5), 1357–1384. https://doi.org/10.1039/C9CS00911F.
(42) Wu, M.; Shan, Z.; Wang, J.; Gu, Z.; Wu, X.; Xu, B.; Zhang, G. Three-Dimensional Covalent Organic Frameworks Based on a π-Conjugated Tetrahedral Node. *Chem. Commun.* **2021**, *57* (80), 10379–10382. https://doi.org/10.1039/D1CC03219D.
(43) Park, J. G.; Aubrey, M. L.; Oktawiec, J.; Chakarawet, K.; Darago, L. E.; Grandjean, F.; Long, G. J.; Long, J. R. Charge Delocalization and Bulk Electronic Conductivity in the Mixed-Valence Metal–Organic Framework Fe(1,2,3-Triazolate)$_2$(BF_4)$_x$. *J. Am. Chem. Soc.* **2018**, *140* (27), 8526–8534. https://doi.org/10.1021/jacs.8b03696.

(44) Chen, G.; Gee, L. B.; Xu, W.; Zhu, Y.; Lezama-Pacheco, J. S.; Huang, Z.; Li, Z.; Babicz, J. T.; Choudhury, S.; Chang, T.-H.; Reed, E.; Solomon, E. I.; Bao, Z. Valence-Dependent Electrical Conductivity in a 3D Tetrahydroxyquinone-Based Metal–Organic Framework. *J. Am. Chem. Soc.* **2020**, *142* (51), 21243–21248. https://doi.org/10.1021/jacs.0c09379.

(45) Wang, S.; Da, L.; Hao, J.; Li, J.; Wang, M.; Huang, Y.; Li, Z.; Liu, Z.; Cao, D. A Fully Conjugated 3D Covalent Organic Framework Exhibiting Band-like Transport with Ultrahigh Electron Mobility. *Angew. Chem. Int. Ed.* **2021**, *60* (17), 9321–9325. https://doi.org/10.1002/anie.202100464.

(46) Koschmieder, S. U.; Wilkinson, G. Homoleptic and Related Aryls of Transition Metals. *Polyhedron* **1991**, *10* (2), 135–173.

(47) Olivar, C.; Parr, J. M.; Avedian, C.; Saal, T.; Zagami, L.; Haiges, R.; Sharma, M.; Inkpen, M. S. Osmium(IV) Tetraaryl Complexes Formed from Prefunctionalized Ligands. *Inorg. Chem.* **2025**, *64* (12), 6192–6204. https://doi.org/10.1021/acs.inorgchem.4c05589.

(48) Zagami, L.; Saal, T.; Avedian, C.; Inkpen, M. S. Intervalence Charge Transfer in an Osmium(IV) Tetra(Ferrocenylaryl) Complex. *Inorg. Chem.* **2025**, *64* (5), 2312–2320.

(49) Tooze, R. P.; Stavropoulos, P.; Motevalli, M.; Hursthouse, M. B.; Wilkinson, G. Synthesis and X-Ray Crystal Structures of the First Tetrahedral Osmium(IV) Compounds, Tetrakis(Cyclohexyl)Osmium(IV) and Tetrakis(o-Methylphenyl)Osmium(IV). J. Chem. Soc., Chem. Commun. 1985, 1139. https://doi.org/10.1039/c39850001139.

(50) Arnold, J.; Wilkinson, G.; Hussain, B.; Hursthouse, M. B. Reactivity of the Homoleptic Osmium Aryl Os(2-MeC6H4)4: Ligand-Induced Reductive Coupling, .Sigma.- to .Pi.-Rearrangement, and Ortho-Hydrogen Activation. *Organometallics* **1989**, *8* (5), 1362–1369. https://doi.org/10.1021/om00107a035.

(51) Lau, M.-K.; Zhang, Q.-F.; Chim, J. L. C.; Wong, W.-T.; Leung, W.-H. Direct Functionalisation of σ-Aryl Ligands: Preparation of Homoleptic Functionalised Aryls of Osmium(Iv). *Chem. Commun.* **2001**, *79* (16), 1478–1479. https://doi.org/10.1039/b104075h.

(52) Parr, J. M.; Olivar, C.; Saal, T.; Haiges, R.; Inkpen, M. S. Pushing Steric Limits in Osmium(IV) Tetraaryl Complexes. *Dalton Trans.* **2022**, *51*, 10558–10570. https://doi.org/10.1039/d2dt01706g.

(53) Arnold, J.; Wilkinson, G.; Hussain, B.; Hursthouse, M. B. Redox Chemistry of the Homoleptic Aryl Os(2-$MeC_6H_4)_4$: Synthesis and Characterization of the First Osmium(v) Organometallic [Os(2-$MeC_6H_4)_4$][CF_3SO_3]. *J Chem Soc Chem Commun* **1988**, *20*, 1349–1350.

(54) Gray, H. B. Molecular Orbital Theory for Transition Metal Complexes. *J. Chem. Educ.* **1964**, *41* (1), 2. https://doi.org/10.1021/ed041p2.

(55) Tanaka, Y.; Kiguchi, M.; Akita, M. Inorganic and Organometallic Molecular Wires for Single-Molecule Devices. *Chem. Eur. J.* **2017**, *23* (20), 4741–4749. https://doi.org/10.1002/chem.201604812.

(56) Vezzoli, A. Metal Complexes and Clusters in Single-Molecule Electronics. In *Encyclopedia of Inorganic and Bioinorganic Chemistry*; Scott, R. A., Ed.; Wiley, 2021; pp 1–21. https://doi.org/10.1002/9781119951438.eibc2787.

(57) Deng, J.-R.; González, M. T.; Zhu, H.; Anderson, H. L.; Leary, E. Ballistic Conductance through Porphyrin Nanoribbons. *J. Am. Chem. Soc.* **2024**, *146* (6), 3651–3659. https://doi.org/10.1021/jacs.3c07734.

(58) Leary, E.; Limburg, B.; Alanazy, A.; Sangtarash, S.; Grace, I.; Swada, K.; Esdaile, L. J.; Noori, M.; González, M. T.; Rubio-Bollinger, G.; Sadeghi, H.; Hodgson, A.; Agraït, N.;

Higgins, S. J.; Lambert, C. J.; Anderson, H. L.; Nichols, R. J. Bias-Driven Conductance Increase with Length in Porphyrin Tapes. *J. Am. Chem. Soc.* **2018**, *140* (40), 12877–12883. https://doi.org/10.1021/jacs.8b06338.

(59) Lovat, G.; Choi, B.; Paley, D. W.; Steigerwald, M. L.; Venkataraman, L.; Roy, X. Room-Temperature Current Blockade in Atomically Defined Single-Cluster Junctions. *Nat. Nanotechnol.* **2017**, *12*, 1050–1054.

(60) Kim, B.; Beebe, J. M.; Olivier, C.; Rigaut, S.; Touchard, D.; Kushmerick, J. G.; Zhu, X.-Y.; Frisbie, C. D. Temperature and Length Dependence of Charge Transport in Redox-Active Molecular Wires Incorporating Ruthenium(II) Bis(Sigma-Arylacetylide) Complexes. *J Phys Chem C* **2007**, *111* (20), 7521–7526.

(61) Lee, W.; Li, L.; Camarasa-Gómez, M.; Hernangómez-Pérez, D.; Roy, X.; Evers, F.; Inkpen, M. S.; Venkataraman, L. Photooxidation Driven Formation of Fe-Au Linked Ferrocene-Based Single-Molecule Junctions. *Nat. Commun.* **2024**, *15* (1), 1439. https://doi.org/10.1038/s41467-024-45707-z.

(62) Skipper, H. E.; May, C. V.; Rheingold, A. L.; Doerrer, L. H.; Kamenetska, M. Hard–Soft Chemistry Design Principles for Predictive Assembly of Single Molecule-Metal Junctions. *J. Am. Chem. Soc.* **2021**, *143* (40), 16439–16447. https://doi.org/10.1021/jacs.1c05142.

(63) Prana, J.; Zagami, L.; Yan, K.; Hernangómez-Pérez, D.; Camarasa-Gómez, M.; Inkpen, M. S. Forming Chemisorbed Single-Molecule Junctions through Loss of Stable Carbocations. *Nano Lett.* **2025**, acs.nanolett.5c01893. https://doi.org/10.1021/acs.nanolett.5c01893.

(64) Olah, G. A. Carbocations and Electrophilic Reactions. *Angew. Chem. Int. Ed. Engl.* **1973**, *12* (3), 173–212. https://doi.org/10.1002/anie.197301731.

(65) Yang, J.; He, W.; Denman, K.; Jiang, Y. B.; Qin, Y. A Molecular Breakwater-like Tetrapod for Organic Solar Cells. *J. Mater. Chem. A* **2015**, *3* (5), 2108–2119. https://doi.org/10.1039/c4ta05405a.

(66) Doud, E. A.; Inkpen, M. S.; Lovat, G.; Montes, E.; Paley, D. W.; Steigerwald, M. L.; Vázquez, H.; Venkataraman, L.; Roy, X. In Situ Formation of N-Heterocyclic Carbene-Bound Single-Molecule Junctions. *J. Am. Chem. Soc.* **2018**, *140* (28), 8944–8949. https://doi.org/10.1021/jacs.8b05184.

(67) Arnold, J.; Wilkinson, G.; Hussain, B.; Hursthouse, M. B. Synthesis and X-Ray Crystal Structure of Tetra(2-Methylphenyl)Molybdenum(IV), $Mo(2\text{-}MeC_6H_4)_4$. Redox Chemistry of $M(2\text{-}MeC_6H_4)_4$ Compounds of Molybdenum, Rhenium, Ruthenium, and Osmium. *Dalton Trans.* **1989**, *11*, 2149. https://doi.org/10.1039/dt9890002149.

(68) Lau, M.-K.; Chim, J. L.; Wong, W.-T.; Williams, I. D.; Leung, W.-H. Synthesis and Molecular Structures of Monooxo Aryl Complexes of Osmium(VI). *Can. J. Chem.* **2001**, *79* (5–6), 607–612. https://doi.org/10.1139/v00-192.

(69) Hardy, D. T.; Wilkinson, G.; Young, G. B. Mechanistic Studies of Ligand-Induced Thermolytic Reductive Elimination of Biaryl from Tetraarylosmium(IV). *Polyhedron* **1996**, *15* (8), 1363–1373. https://doi.org/10.1016/0277-5387(95)00364-9.

(70) Larsen, E.; La Mar, G. N. The Angular Overlap Model. How to Use It and Why. *J. Chem. Educ.* **1974**, *51* (10), 633. https://doi.org/10.1021/ed051p633.

(71) Venkataraman, L.; Klare, J. E.; Tam, I. W.; Nuckolls, C.; Hybertsen, M. S.; Steigerwald, M. L. Single-Molecule Circuits with Well-Defined Molecular Conductance. *Nano Lett.* **2006**, *6* (3), 458–462. https://doi.org/10.1021/nl052373+.

(72) Yanson, A. I.; Rubio Bollinger, G.; Van Den Brom, H. E.; Agraït, N.; Van Ruitenbeek, J. M. Formation and Manipulation of a Metallic Wire of Single Gold Atoms. *Nature* **1998**, *395* (6704), 783–785. https://doi.org/10.1038/27405.

(73) Quek, S. Y.; Kamenetska, M.; Steigerwald, M. L.; Choi, H. J.; Louie, S. G.; Hybertsen, M. S.; Neaton, J. B.; Venkataraman, L. Mechanically Controlled Binary Conductance Switching of a Single-Molecule Junction. *Nat. Nanotechnol.* **2009**, *4* (4), 230–234. https://doi.org/10.1038/nnano.2009.10.
(74) Klausen, R. S.; Widawsky, J. R.; Steigerwald, M. L.; Venkataraman, L.; Nuckolls, C. Conductive Molecular Silicon. *J. Am. Chem. Soc.* **2012**, *134* (10), 4541–4544. https://doi.org/10.1021/ja211677q.
(75) Stavropoulos, P.; Savage, P. D.; Tooze, R. P.; Wilkinson, G.; Hussain, B.; Motevalli, M.; Hursthouse, M. B. The Synthesis and X-Ray Crystal Structures of Homoleptic Tetrahedral Aryls of Osmium(IV) and of Cyclohexyls of Ruthenium(IV), Osmium(IV), and Chromium(IV). *Dalton Trans.* **1987**, *3*, 557.
(76) Quek, S. Y.; Choi, H. J.; Louie, S. G.; Neaton, J. B. Length Dependence of Conductance in Aromatic Single-Molecule Junctions. *Nano Lett.* **2009**, *9* (11), 3949–3953. https://doi.org/10.1021/nl9021336.
(77) Olah, G. A. Stable Carbonium Ions in Solution. *Science* **1970**, *168* (3937), 1298–1311.
(78) Kim, K.-C.; Reed, C. A.; Elliott, D. W.; Mueller, L. J.; Tham, F.; Lin, L.; Lambert, J. B. Crystallographic Evidence for a Free Silylium Ion. *Science* **2002**, *297* (5582), 825–827. https://doi.org/10.1126/science.1073540.
(79) Prana, J.; Kim, L.; Czyszczon-Burton, T.; Homann, G.; Chen, S.; Miao, Z.; Camarasa-Gomez, M.; Inkpen, M. Lewis-Acid Mediated Reactivity in Single-Molecule Junctions. *J Am Chem Soc* **2024**, *146* (48), 33265–33275. https://doi.org/10.1021/jacs.4c14176.
(80) Ghasemi, S.; Ornago, L.; Liasi, Z.; Johansen, M. B.; Von Buchwald, T. J.; Hillers-Bendtsen, A. E.; Van Der Poel, S.; Hölzel, H.; Wang, Z.; Amombo Noa, F. M.; Öhrström, L.; Mikkelsen, K. V.; Van Der Zant, H. S. J.; Lara-Avila, S.; Moth-Poulsen, K. Exploring the Impact of Select Anchor Groups for Norbornadiene/Quadricyclane Single-Molecule Switches. *J. Mater. Chem. C* **2023**, *11* (44), 15412–15418. https://doi.org/10.1039/D3TC02652C.
(81) Meisner, J. S.; Ahn, S.; Aradhya, S. V.; Krikorian, M.; Parameswaran, R.; Steigerwald, M.; Venkataraman, L.; Nuckolls, C. Importance of Direct Metal−π Coupling in Electronic Transport Through Conjugated Single-Molecule Junctions. *J. Am. Chem. Soc.* **2012**, *134* (50), 20440–20445. https://doi.org/10.1021/ja308626m.
(82) Su, T. A.; Li, H.; Klausen, R. S.; Widawsky, J. R.; Batra, A.; Steigerwald, M. L.; Venkataraman, L.; Nuckolls, C. Tuning Conductance in π–σ–π Single-Molecule Wires. *J. Am. Chem. Soc.* **2016**, *138*, 7791–7795.
(83) Fatemi, V.; Kamenetska, M.; Neaton, J. B.; Venkataraman, L. Environmental Control of Single-Molecule Junction Transport. *Nano Lett.* **2011**, *11* (5), 1988–1992. https://doi.org/10.1021/nl200324e.
(84) Kawai, S. Discussion on Decomposition of Chloroform. *Yakugaku Zasshi* **1966**, *86* (12), 1125–1132. https://doi.org/10.1248/yakushi1947.86.12_1125.
(85) Traverso, O.; Scandola, F. Photooxidation of Ferrocene in Halocarbon Solvents. *Inorganica Chim. Acta* **1970**, *4*, 493–498. https://doi.org/10.1016/S0020-1693(00)93335-8.
(86) Nagahara, L. A.; Thundat, T.; Lindsay, S. M. Preparation and Characterization of STM Tips for Electrochemical Studies. *Rev. Sci. Instrum.* **1989**, *60* (10), 3128–3130. https://doi.org/10.1063/1.1140590.
(87) Capozzi, B.; Low, J. Z.; Xia, J.; Liu, Z.-F.; Neaton, J. B.; Campos, L. M.; Venkataraman, L. Mapping the Transmission Functions of Single-Molecule Junctions. *Nano Lett.* **2016**, *16* (6), 3949–3954. https://doi.org/10.1021/acs.nanolett.6b01592.

(88) Low, J. Z.; Capozzi, B.; Cui, J.; Wei, S.; Venkataraman, L.; Campos, L. M. Tuning the Polarity of Charge Carriers Using Electron Deficient Thiophenes. *Chem. Sci.* **2017**, *8* (4), 3254–3259. https://doi.org/10.1039/c6sc05283e.
(89) Capozzi, B.; Xia, J.; Adak, O.; Dell, E. J.; Liu, Z.-F.; Taylor, J. C.; Neaton, J. B.; Campos, L. M.; Venkataraman, L. Single-Molecule Diodes with High Rectification Ratios through Environmental Control. *Nat. Nanotechnol.* **2015**, *10* (6), 522–527. https://doi.org/10.1038/nnano.2015.97.
(90) Blum, V.; Gehrke, R.; Hanke, F.; Havu, P.; Havu, V.; Ren, X.; Reuter, K.; Scheffler, M. Ab Initio Molecular Simulations with Numeric Atom-Centered Orbitals. *Comput. Phys. Commun.* **2009**, *180* (11), 2175–2196. https://doi.org/10.1016/j.cpc.2009.06.022.
(91) Camarasa-Gómez, M.; Hernangómez-Pérez, D.; Wilhelm, J.; Bagrets, A.; Evers, F. Molecular Transport, in J. W. Abbot, C. M. Acosta, A. Akoush, [and 199 others in alphabetical order], Roadmap for Advancements of the FHI-aims Software Package, arXiv, Submission Date: 2025-04-30. DOI: 10.48550/arXiv.2505.00125 (accessed 2025-07-05).
(92) Camarasa-Gómez, M.; Hernangómez-Pérez, D.; Evers, F. Spin–Orbit Torque in Single-Molecule Junctions from Ab Initio. *J. Phys. Chem. Lett.* **2024**, *15* (21), 5747–5753.
(93) Arnold, A.; Weigend, F.; Evers, F. Quantum Chemistry Calculations for Molecules Coupled to Reservoirs: Formalism, Implementation, and Application to Benzenedithiol. *J. Chem. Phys.* **2007**, *126* (17), 174101. https://doi.org/10.1063/1.2716664.
(94) Bagrets, A. Spin-Polarized Electron Transport Across Metal–Organic Molecules: A Density Functional Theory Approach. *J. Chem. Theory Comput.* **2013**, *9* (6), 2801–2815. https://doi.org/10.1021/ct4000263.
(95) Perdew, J. P.; Burke, K.; Ernzerhof, M. Generalized Gradient Approximation Made Simple. *Phys. Rev. Lett.* **1996**, *77* (18), 3865–3868. https://doi.org/10.1103/PhysRevLett.77.3865.
(96) Evers, F.; Korytár, R.; Tewari, S.; Van Ruitenbeek, J. M. Advances and Challenges in Single-Molecule Electron Transport. *Rev. Mod. Phys.* **2020**, *92* (3), 35001. https://doi.org/10.1103/RevModPhys.92.035001.
(97) Thoss, M.; Evers, F. Perspective: Theory of Quantum Transport in Molecular Junctions. *J. Chem. Phys.* **2018**, *148* (3), 30901. https://doi.org/10.1063/1.5003306.
(98) Prindle, C. R.; Shi, W.; Li, L.; Jensen, J. D.; Laursen, B. W.; Steigerwald, M. L.; Nuckolls, C.; Venkataraman, L. Effective Gating in Single-Molecule Junctions through Fano Resonances. *J. Am. Chem. Soc.* **2024**, *146*, 3646-3650. https://doi.org/10.1021/jacs.3c14226.
(99) Lambert, C. J.; Osikowicz, W.; Wang, Y.; Salaneck, W. R.; Mishchenko, A.; Wandlowski, T.; Mayor, M.; Schoen, G.; Pauly, F.; Neaton, J. B.; Macdonald, J. E.; Nichols, R. J. Basic Concepts of Quantum Interference and Electron Transport in Single-Molecule Electronics. *Chem. Soc. Rev.* **2015**, *44* (4), 875–888. https://doi.org/10.1039/C4CS00203B.
(100) Venkataraman, L.; Park, Y. S.; Whalley, A. C.; Nuckolls, C.; Hybertsen, M. S.; Steigerwald, M. L. Electronics and Chemistry: Varying Single-Molecule Junction Conductance Using Chemical Substituents. *Nano Lett.* **2007**, *7* (2), 502–506. https://doi.org/10.1021/nl062923j.
(101) Paier, J.; Marsman, M.; Kresse, G. Why Does the B3LYP Hybrid Functional Fail for Metals? *J. Chem. Phys.* **2007**, *127* (2). https://doi.org/10.1063/1.2747249.
(102) Edwards, P. G.; Behling, T.; Wilkinson, G.; Motevalli, M.; Hursthouse, M. B. Oxoaryls of Rhenium-(V) and -(VI) and Osmium(VI). X-Ray Crystal Structures of Dimesityldioxorhenium(VI), Tetramesityloxorhenium(VI), and Dimesityldioxoosmium(VI). *J. Chem. Soc. Dalton Trans.* **1987**, 169–175.

For Table of Contents Only